Neurobiology of Disease 206 (2025) 106802

Contents lists available at ScienceDirect

Neurobiology of Disease

journal homepage: www.elsevier.com/locate/ynbdi

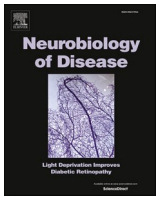

The brain interactome of a permissive prion replication substrate

Hamza Arshad [a,b], Shehab Eid [a,c], Surabhi Mehra [a], Declan Williams [a], Lech Kaczmarczyk [d,e], Erica Stuart [a], Walker S. Jackson [d,e], Gerold Schmitt-Ulms [a,c], Joel C. Watts [a,b,*]

[a] Tanz Centre for Research in Neurodegenerative Diseases, University of Toronto, Toronto, Ontario, Canada
[b] Department of Biochemistry, University of Toronto, Toronto, Ontario, Canada
[c] Department of Laboratory Medicine and Pathobiology, University of Toronto, Toronto, Ontario, Canada
[d] Wallenberg Center for Molecular Medicine, Department of Biomedical and Clinical Sciences, Linköping University, Linköping, Sweden
[e] German Center for Neurodegenerative Diseases (DZNE), Bonn, Germany

ARTICLE INFO

Keywords:
Prion
Protein-protein interactions
Mass spectrometry
Knock-in mice
Bank voles

ABSTRACT

Bank voles are susceptible to prion strains from many different species, yet the molecular mechanisms underlying the ability of bank vole prion protein (BVPrP) to function as a universal prion acceptor remain unclear. Potential differences in molecular environments and protein interaction networks on the cell surface of brain cells may contribute to BVPrP's unusual behavior. To test this hypothesis, we generated knock-in mice that express physiological levels of BVPrP (M109 isoform) and employed mass spectrometry to compare the interactomes of mouse (Mo) PrP and BVPrP following mild in vivo crosslinking of brain tissue. Substantial overlap was observed between the top interactors for BVPrP and MoPrP, with established PrP-interactors such as neural cell adhesion molecules, subunits of Na^+/K^+-ATPases, and contactin-1 being equally present in the two interactomes. We conclude that the molecular environments of BVPrP and MoPrP in the brains of mice are very similar. This suggests that the unorthodox properties of BVPrP are unlikely to be mediated by differential interactions with other proteins.

1. Introduction

Prion diseases such as scrapie in sheep, bovine spongiform encephalopathy, chronic wasting disease (CWD) in cervids, and Creutzfeldt-Jakob disease (CJD) in humans are caused by the accumulation of misfolded prion protein (PrP) in the brain. Encoded by the *Prnp* gene in rodents, PrP is a glycosylphosphatidylinositol (GPI)-anchored protein present on the cell surface of neurons and astrocytes that is modified post-translationally by the addition of up to two N-linked glycans. During prion disease, PrP undergoes conversion from its normal, cellular form (PrP^C) into a self-propagating, aggregation-prone conformer termed PrP^{Sc} (Colby and Prusiner, 2011). These two PrP conformers have distinct physicochemical properties: PrP^C is predominantly α-helical and sensitive to digestion with proteases whereas PrP^{Sc} is composed almost entirely of β-sheets and, due to its aggregated nature, is partially resistant to digestion with proteases such as proteinase K (Kraus et al., 2021; Manka et al., 2022; McKinley et al., 1983; Riek et al., 1996). Prion diseases are transmissible, as an exogenous source of PrP^{Sc} can template the conversion of host expressed PrP^C into additional copies of PrP^{Sc}, allowing prions to spread both within and to the brain via a cascade of protein misfolding. PrP^C expression is necessary for both prion replication and prion neurotoxicity (Brandner et al., 1996a; Brandner et al., 1996b; Bueler et al., 1993; Fang et al., 2016). Prion disease pathogenesis likely stems directly from PrP^{Sc} accumulation or prion replication rather than loss of PrP^C since PrP knockout ($PrP^{-/-}$) mice do not develop signs of prion disease during their lifespans (Bueler et al., 1992).

While intraspecies prion transmission is generally efficient, cross-species transmission is typically an inefficient process characterized by incomplete disease transmission and prolonged incubation periods. This phenomenon, known as the "species barrier", is mediated by both amino acid sequence differences between PrP^{Sc} and PrP^C as well as structural compatibility between the two molecules (Collinge and Clarke, 2007; Prusiner et al., 1990; Scott et al., 1989). Bank voles (*Myodes glareolus*) are atypical in that they do not impose a substantial species barrier during prion transmission and are highly susceptible to prions from many different species (Agrimi et al., 2008; Arshad et al., 2020; Di Bari et al., 2013; Nonno et al., 2006; Nonno et al., 2020; Nonno et al., 2019; Pirisinu et al., 2016; Pirisinu et al., 2022). Transgenic or knock-in mice

* Corresponding author at: Krembil Discovery Tower, Rm. 4KD481, 60 Leonard Ave., Toronto M5T 0S8, Ontario, Canada.
E-mail address: joel.watts@utoronto.ca (J.C. Watts).

https://doi.org/10.1016/j.nbd.2025.106802
Received 18 September 2024; Received in revised form 10 December 2024; Accepted 9 January 2025
Available online 10 January 2025

expressing bank vole PrP (BVPrP) recapitulate the enhanced prion susceptibility of bank voles, indicating that this phenomenon is mediated by BVPrP itself (Espinosa et al., 2016; Kobayashi et al., 2019; Watts et al., 2014). Moreover, BVPrP functions as a highly permissive prion substrate when expressed in cultured cells or used for in vitro prion conversion assays (Arshad et al., 2023; Burke et al., 2020; Cosseddu et al., 2011; Erana et al., 2019; Mok et al., 2021; Orru et al., 2015; Schwenke et al., 2022). Collectively, these results suggest that BVPrP may be capable of functioning as a "universal acceptor" for prions.

A molecular explanation for the enhanced ability of BVPrP to mediate cross-species prion transmission remains to be fully determined. The sequence of mature BVPrP, following removal of N- and C-terminal signal sequences, differs from that of mouse PrP (MoPrP) at only eight positions, suggesting that a small number of residues can have a large effect on the properties of the protein. Indeed, the ability of BVPrP to enable replication of both mouse and hamster prion strains is governed by five key residues (Arshad et al., 2024). Additionally, BVPrP is polymorphic at codon 109, where either a methionine (M109) or isoleucine (I109) residue can be present (Cartoni et al., 2005). Transgenic mice over-expressing wild-type (WT) or mutant BVPrP(I109) as well as knock-in mice expressing physiological levels of mutant BVPrP(I109) develop spontaneous disease that exhibits many of the hallmarks of authentic prion disease, suggesting that BVPrP may be intrinsically prone to adopting misfolded conformations (Mehra et al., 2024; Otero et al., 2019; Walsh et al., 2024; Watts et al., 2016; Watts et al., 2012).

The issue of whether proteins other than PrP participate in prion replication in vivo remains an open question (Eid et al., 2024). Non-protein cofactors such as polyanions and specific lipids can modulate prion replication and the properties of prion strains in vitro (Burke et al., 2019; Deleault et al., 2003; Deleault et al., 2012a; Deleault et al., 2012b; Fernandez-Borges et al., 2018). Based on prion transmission experiments, it has been hypothesized that a PrP-interacting protein, provisionally designated "Protein X", may be required for prion replication (Kaneko et al., 1997; Telling et al., 1995). Indeed, PrP^{C} is known to interact with a number of other cell membrane proteins including neural cell adhesion molecule (NCAM1 and NCAM2) (Santuccione et al., 2005; Schmitt-Ulms et al., 2001), subunits of Na^{+}/K^{+}-ATPases (NKAs) (Kleene et al., 2007; Williams et al., 2021), dipeptidyl aminopeptidase-like protein 6 (DPP6) (Mercer et al., 2013), the laminin receptor (Rieger et al., 1997), and G protein-couple receptor 126 (Gpr126, also known as Adgrg6) (Kuffer et al., 2016). Interactome experiments have revealed many more proteins residing in close spatial proximity to PrP^{C} within the membrane (Ghodrati et al., 2018; Rutishauser et al., 2009; Schmitt-Ulms et al., 2004; Ulbrich et al., 2018; Watts et al., 2009; Williams et al., 2021; Zafar et al., 2017). Only a few identified PrP^{C}-interacting proteins have been demonstrated to modulate the conversion of PrP^{C} into PrP^{Sc}. For instance, the prion protein family member Shadoo interacts with PrP^{C} and has been shown to increase PrP^{Sc} formation in cultured cells, although Shadoo levels do not appear to affect the kinetics of prion replication in mice (Ciric et al., 2015; Daude et al., 2012; Watts et al., 2011). Conversely, the 14–3-3β protein interacts with PrP^{C} and disaggregates fibrils formed by a peptide consisting of PrP residues 106–126 (Han et al., 2014). While PrP^{C}-interacting proteins have yet to provide conclusive insight into the mechanism of prion replication, they have revealed that PrP^{C} may influence multiple biological processes within the cell (Schmitt-Ulms et al., 2021; Watts et al., 2018).

We hypothesized that due to its unique amino acid composition, BVPrP may interact with a distinct set of proteins in the brain compared to MoPrP, and that this may in part explain the ability of BVPrP to promote cross-species prion transmission. To address this issue experimentally, we compared the interactomes of MoPrP and BVPrP using healthy WT C57BL/6 mice expressing MoPrP and knock-in mice expressing BVPrP(M109), termed kiBVM mice. Qualitative and quantitative mass spectrometry experiments revealed that the molecular environments of MoPrP and BVPrP within the brain are very similar, arguing that intrinsic biophysical features of BVPrP rather than altered protein-protein interactions drive the ability of BVPrP to function as a universal prion acceptor.

2. Methods

2.1. Mice

Non-transgenic C57BL/6 mice were bred in-house and were originally sourced from Jackson Lab (Stock #000664). B6(Cg)-*Tyr*$^{c\text{-}2J}$/J mice ("B6-albino"; Stock #000058) and B6.129S4-*Gt(ROSA)26Sor*$^{tm1(FLP1)Dym}$/RainJ mice ("Flp deleter"; Stock #009086) were also purchased from Jackson Lab. $PrP^{-/-}$ mice on a C57BL/6 co-isogenic background were provided by Adriano Aguzzi (Nuvolone et al., 2016). Mice were housed in cages of 3–5 animals and were given free access to food and water. The mice were maintained on a 12 h light / 12 h dark cycle. Mice were monitored daily for routine health and checked biweekly for signs of neurological illness as previously described (Mehra et al., 2024). All animal experiments were conducted under an animal use protocol approved by the University Health Network Animal Care Committee (#AUP4263.19).

2.2. Generation of BVPrP knock-in mice

The open reading frame of BVPrP(M109) (GenBank accession numbers AF367624.1 and EF455012.1) was synthesized and then amplified by PCR using the primers 5'-CTATATGGATCCACCATGGCGAACCTCAGC-3′ (forward) 5′- CTATATTCTAGATCATCCCACGATCAGGAAG-3′ (reverse) for insertion between the *BamH*I and *Xba*I sites of the vector pcDNA3. Generation of the targeting constructs as well as gene targeting of the *Prnp* locus in mouse V6.5 embryonic stem cells using CRISPR/Cas9 technology were performed as described previously (Kaczmarczyk et al., 2016; Mehra et al., 2024). Clones with successful gene targeting were expanded and aggregated with diploid CD-1(ICR) mouse embryos at The Centre for Phenogenomics (Toronto, Canada). Chimeric mice were identified by the presence of black patches of fur and were then bred with B6-albino mice to identify those that underwent germline transmission events. The chimeric mice were then bred with Flp deleter mice to remove the selectable marker, and then the offspring of this cross were bred with WT C57BL/6 mice to eliminate the Flp allele. These mice were then intercrossed to generate homozygous knock-in mice. The knock-in mice were maintained by crossing homozygous female with homozygous male mice.

2.3. Tissue harvesting and homogenization

WT C57BL/6 and kiBVM mice at 3–4 months of age were perfused with PBS for 2 min and then brain, spinal cord, heart, lung, muscle, testis, tongue, skin, stomach, and spleen tissue was harvested and snap frozen in liquid nitrogen, followed by storage at −80 °C. Tissues were weighed and then placed in screw cap tubes containing 0.5 mm zirconia beads (BioSpec #11079105Z). Nine volumes of PBS were added to generate 10 % (w/v) homogenates. Samples were homogenized three times for 3 min each using a Minilys homogenizer (Bertin Technologies) set at maximum speed, with 5 min incubations on ice in between runs. Some organs such as skin and stomach required additional homogenization to fully break up the tissue. Detergent-extracted homogenates were generated by mixing 9 volumes of 10 % tissue homogenate with 1 volume of 10× detergent buffer [5 % (w/v) sodium deoxycholate, 5 % (*v*/v) NP-40 in 1× PBS]. Samples were incubated on ice for 10 min with intermittent vortexing to promote efficient protein extraction and then centrifuged at 5,000 ×*g* for 5 min at 4 °C. The bicinchoninic acid (BCA) assay (Thermo Fisher #23227) was used to determine total protein concentrations in the detergent-extracted tissue homogenates.

2.4. Detergent insolubility assays and thermolysin digestions

To generate detergent-insoluble fractions, detergent-extracted brain homogenates were diluted in 1× detergent buffer [0.5 % (w/v) sodium deoxycholate, 0.5 % (v/v) NP-40 prepared in DPBS] and then subjected to ultracentrifugation at 100,000 ×*g* in a Beckman TLA-55 rotor for 1 h at 4 °C. Supernatants were removed and then pellets were resuspended in 1× Bolt LDS sample buffer (Thermo Fisher #B0007) containing 2.5 % (v/v) β-mercaptoethanol. The samples were boiled at 95 °C for 10 min and then analyzed by immunoblotting. For thermolysin digestions, 500 μg of detergent-extracted brain homogenate was added to 1× detergent buffer (final volume: 100 μL) containing 50 μg/mL thermolysin (MilliporeSigma #T7902; diluted from a 1 mg/mL stock solution prepared in dH_2O). This results in a protease:protein ratio of 1:100 in the final reaction. Samples were incubated at 37 °C for 1 h with 600 rpm shaking, and digestions were halted by adding EDTA to a final concentration of 5 mM. Sarkosyl was added to a final concentration of 2 % (v/v), and then samples were ultracentrifuged at 100,000 ×*g* for 1 h at 4 °C. Supernatants were gently removed and then pellets were resuspended in 1× Bolt LDS sample buffer containing 2.5 % (v/v) β-mercaptoethanol, boiled, and analyzed by immunoblotting.

2.5. De-glycosylation of proteins using PNGase F

Detergent-extracted brain homogenates containing 100 μg of protein were incubated at 95 °C for 10 min following addition of one volume of 10× glycoprotein denaturing buffer. The samples were cooled on ice, and then 5 μL of 10 % NP-40 and 10× GlycoBuffer 2 as well as 1 μL of PNGase F (New England Biolabs #P0704S) were added to make a final reaction volume of 50 μL. Following overnight incubation at 37 °C, reactions were stopped by adding LDS sample buffer (1× final concentration) and boiling the samples at 95 °C for 10 min. De-glycosylated samples were analyzed by immunoblotting.

2.6. Immunoblotting

Samples were run on 10 % Bolt Bis-Tris gels (Thermo Fisher #NW00100BOX or NW00102BOX) at 165 V for 35 min. Gels were transferred onto a 0.45 μm Immobilon-P PVDF membranes (MilliporeSigma #IPVH00010) using Tris-Glycine transfer buffer (100 mM Tris-HCl pH 8, 137 mM glycine) at 25 V for 60 min. Following transfer, membranes were blocked for 1 h in blocking buffer [5 % (w/v) skim milk in Tris-buffered saline (TBS) containing 0.05 % (v/v) Tween-20 (TBST)]. The blocked membranes were then incubated with primary antibody diluted in blocking buffer overnight at 4 °C. The following primary anti-PrP antibodies were used: HuM-D18 (1:5,000 dilution) (Williamson et al., 1998), HuM-D13 (1:10,000 dilution) (Williamson et al., 1998), POM1 (MilliporeSigma #MABN2285; 1:5,000 dilution) (Polymenidou et al., 2008), HuM-R1 (1:10,000 dilution) (Williamson et al., 1998), SAF-32 (Cayman Chemical #189720; 1:5,000 dilution), and Sha31 (Cayman Chemical #11866; 1:5,000 dilution). The HuM-D18 antibody was produced in-house whereas the HuM-D13 and HuM-R1 antibodies were provided by Stanley Prusiner (University of California San Francisco). The membranes were then washed 3 times with TBST for 10 min each, and then incubated with the appropriate HRP-linked secondary antibody (Bio-Rad #172–1011 or Thermo Fisher Scientific #31414) at a 1:10,000 dilution in blocking buffer for 1 h at 22 °C. Membranes were then washed 3 times with TBST for 10 min and then developed using Western Lightning ECL Pro (Revvity NEL #122001EA) and exposed to x-ray film. For reprobing with an actin antibody, blots were washed with TBST and then treated with 0.05 % (w/v) sodium azide diluted in blocking buffer to inactivate the HRP linked to the initial secondary antibody. Blots were then reprobed using the primary anti-actin 20–33 antibody (MilliporeSigma #A5060; 1:10,000 dilution) and an HRP-linked goat anti-rabbit secondary antibody (Bio-Rad #172–1019). For quantification of PrP levels, immunoblots were scanned and densitometry was performed using ImageJ.

2.7. Time-controlled transcardiac perfusion crosslinking

TcTPC was performed as previously described (Schmitt-Ulms et al., 2004). Briefly, male WT C57BL/6 mice, kiBVM, and $PrP^{-/-}$ mice at approximately 3 months of age were anesthetized with isoflurane and then perfused via the transcardiac route with PBS for 2 min. Following this, mice were perfused with freshly made 2 % (w/v) formaldehyde (pH 7.3 in 1× PBS) for 6 min. Successful perfusion was gauged by the development of tail rigidity. The brains were then dissected and post-fixed in 2 % formaldehyde for a total of 9 min (includes dissection time). Following fixation, brains were snap frozen in liquid nitrogen and stored at −80 °C.

2.8. Immunoprecipitation of crosslinked PrP^C-containing complexes

KappaSelect beads (Cytiva #17–5458-01) were washed, equilibrated, and then conjugated with HuM-D18 Fab by rotation overnight at 4 °C in lysis buffer [150 mM Tris-HCl pH 8.3, 150 mM NaCl, 0.5 % (w/v) deoxycholic acid, 0.5 % (v/v) NP-40]. The crosslinked brains were homogenized as described above in lysis buffer and then ultracentrifuged at 100,000 ×*g* for 1 h at 4 °C to remove debris. The brain homogenates were then quantified using the BCA assay and then normalized to the lowest protein concentration amongst all replicates. Homogenates were then incubated with the HuM-D18-conjugated KappaSelect beads overnight at 4 °C in an end-over-end rotator. Following capture, beads were washed 3 times with lysis buffer and then 3 times with a more stringent lysis buffer containing a higher salt concentration (500 mM NaCl). Prior to elution, beads were washed briefly with a buffer containing 10 mM HEPES, pH 8. Captured proteins were eluted by pH drop using 0.2 % (v/v) trifluoroacetic acid in 20 % (v/v) acetonitrile.

2.9. Sample reduction, alkylation, trypsinization, and iTRAQ labeling

Eluates from the immunoprecipitation of PrP^C-containing complexes were dried to a volume of 5 μL using a SpeedVac centrifuge set at 37 °C. The dried eluates were denatured by addition of 9 M deionized urea and then reduced by incubation with Tris(2-carboxyethyl)phosphine (TCEP) in 500 mM triethyl ammonium bicarbonate buffer at 60 °C for 30 min. After allowing the samples to cool, sulfhydryl groups were alkylated by treatment with 4-vinylpyridine for 1 h at 22 °C. Urea concentration was diluted to 1.25 M in 500 mM triethylammonium bicarbonate buffer prior to the addition of mass spectrometry grade trypsin (Thermo Fisher Scientific #90057). Trypsin digestions were done overnight at 37 °C. The digested mixture was purified with reverse phase resin, paired with or without a strong cation exchange. A portion of the trypsinized samples were reacted with 8-plex iTRAQ reagents (SCIEX #4390811) according to the manufacturer's instructions and then combined. Prior to LC-MS/MS, peptides were purified using OMIX C18 pipette tips (Agilent #A57003100).

2.10. LC-MS/MS analysis

Samples were analyzed using an EASY-nLC 1000-Orbitrap Fusion Tribid mass spectrometry platform (Thermo Fisher Scientific) with a 4-h reversed-phase acetonitrile/water gradient at a flow rate of 300 nL/min. The analytical C18 column (Acclaim PepMap RSLC 100) was 25 cm long with a 75 μm inner diameter. Each LC-MS/MS run consisted of an orbitrap precursor ion scan as well as ion trap (MS2) and orbitrap (MS3) product ion scans within a 3-s window following collision induced dissociation and higher energy collisional dissociation, respectively. For the orbitrap scans, the resolution was set at 60,000.

2.11. Protein identification and quantification

The MS2 data sets were analyzed and converted into peptide sequences with Proteome Discoverer software (version 1.4) using the built-in Mascot and Sequest HT search algorithms and search parameters as previously described (Ghodrati et al., 2018). The mouse Uniprot database was used as a reference with the manual inclusion of the BVPrP sequence. To stringently filter the mass spectra, the Percolator algorithm within Proteome Discoverer was used to estimate the false discovery rate based on the q-value. The Reporter Ions Quantifier algorithm in Proteome Discoverer was utilized to determine the relative quantification of iTRAQ-labeled peptides using the MS3 data. For the unlabeled datasets, the number of PSMs for the 3 biological replicates of the kiBVM samples, the 3 biological replicates of the WT C57BL/6 samples, and the two biological replicates of the $PrP^{-/-}$ samples were averaged for each identified protein. Hits were then sorted by the average number of PSMs in the kiBVM or WT samples minus the average number of PSMs in the $PrP^{-/-}$ samples. For a protein to be included in the list of identified interactors, its identification had to be supported by at least 2 unique peptides as well as an average kiBVM:average $PrP^{-/-}$ or an average WT: average $PrP^{-/-}$ PSM ratio of at least 3.

2.12. Statistical analysis

Statistical comparisons were conducted using GraphPad Prism software (version 10), with a significance threshold of $P < 0.05$. iTRAQ reporter ion enrichment ratios, relative PrP^{C} levels in brain homogenates, and levels of detergent-insoluble PrP were compared using two-tailed Welch's *t*-tests, which do not assume equal standard deviations between sample groups.

3. Results

Previously, we generated knock-in (ki) mice expressing the I109 isoform of BVPrP (Mehra et al., 2024). Lines expressing either WT, D178N-mutant, or E200K-mutant BVPrP(I109) were created, which we termed $kiBVI^{WT}$, $kiBVI^{D178N}$, and $kiBVI^{E200K}$, respectively. Because most studies exploring the ability of BVPrP to function as a universal prion acceptor have utilized the M109 isoform of BVPrP, we decided to generate ki mice expressing WT BVPrP(M109), referred to hereafter as kiBVM mice. To create kiBVM mice, the PrP open reading frame within Exon 3 of mouse *Prnp* was replaced with the corresponding region of bank vole *Prnp*, allowing BVPrP expression to be controlled by the endogenous mouse *Prnp* promoter (Fig. 1A). PrP levels in brain homogenates from kiBVM, WT C57BL/6 mice, and co-isogenic $PrP^{-/-}$ mice on a C57BL/6 background (Nuvolone et al., 2016) were compared by

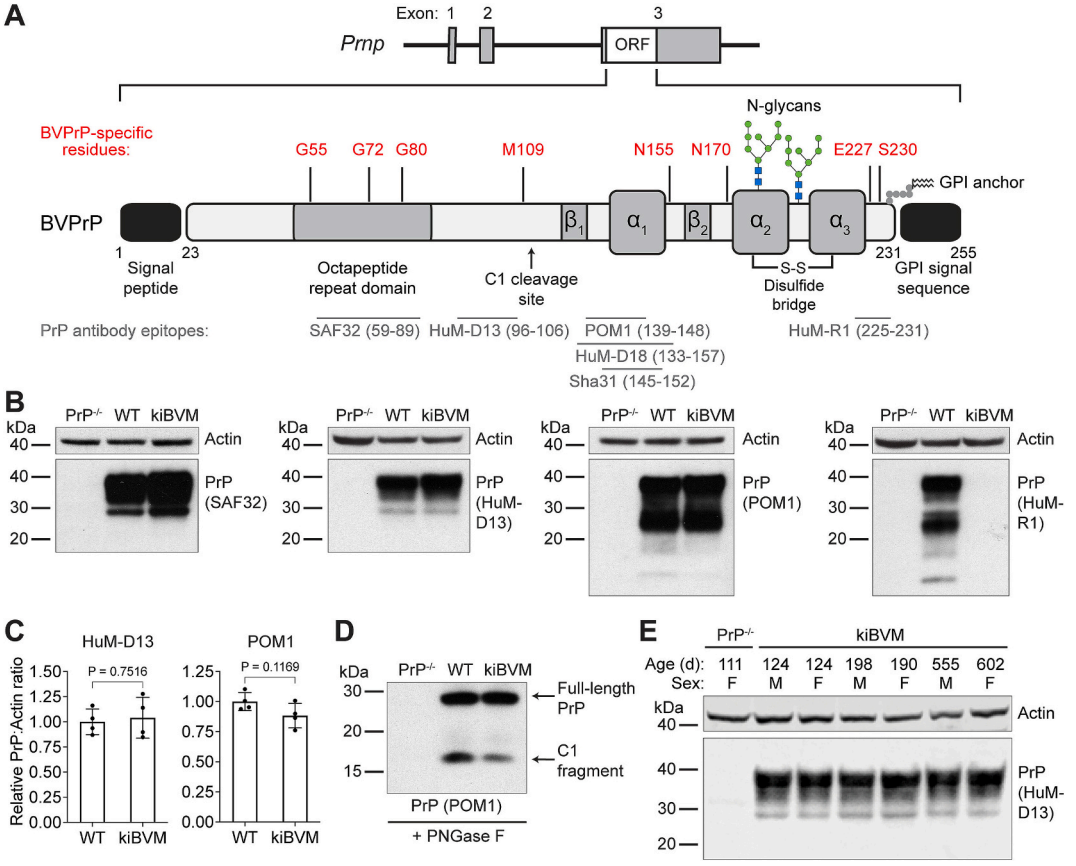

Fig. 1. Generation of knock-in mice expressing bank vole PrP. A) Schematic of the gene-targeted allele in kiBVM mice expressing BVPrP(M109). The eight amino acid residue differences between the mature forms of BVPrP and MoPrP are shown, as are the approximate epitopes for the anti-PrP antibodies used in this study. B) Representative immunoblots for PrP in brain extracts from a $PrP^{-/-}$ mouse, a wild-type C57BL/6 (WT) mouse, and a kiBVM mouse probed with antibodies that recognize both MoPrP and BVPrP (SAF32, HuM-D13, and POM1) or only MoPrP (HuM-R1). Blots were reprobed with an antibody against actin. C) Quantification of PrP^{C} levels in brain homogenates from WT and kiBVM mice ($n = 4$ each), as assessed by immunoblotting using either the HuM-D13 (left graph) or POM1 (right graph) antibodies. Statistical significance was assessed using a two-tailed Welch's *t*-test. D) Immunoblot for PrP in PNGase F-treated brain extracts from a $PrP^{-/-}$ mouse, a WT mouse, and a kiBVM mouse probed with the antibody POM1. Full-length BVPrP as well as the C1 endoproteolytic product are indicated. E) Immunoblot for PrP in brain extracts from kiBVM mice at the indicated ages probed with the antibody HuM-D13. Brains from both male (M) and female (F) mice were analyzed. The blot was reprobed with an antibody against actin.

immunoblotting. Using three different antibodies (SAF32, HuM-D13, and POM1) that recognize different epitopes within PrP (Fig. 1A), the expression level of BVPrP in the brains of kiBVM mice and MoPrP in the brains of WT mice were found to be similar **(**Fig. 1B**).** As expected, the HuM-R1 antibody, which recognizes an epitope uniquely present in the C-terminal region of MoPrP, failed to detect BVPrP in the brains of kiBVM mice. None of the antibodies detected PrP signal in brain homogenates from $PrP^{-/-}$ mice. Quantification of PrP^{C} levels in the brains of WT and kiBVM mice using two distinct antibodies that recognize conserved epitopes in MoPrP and BVPrP revealed no significant differences (Fig. 1C). PrP N-glycosylation patterns, which can influence PrP aggregation (Sevillano et al., 2020), did not appear to be altered in kiBVM mice (Fig. 1B), although we did not compare the carbohydrate composition of the N-glycans linked to PrP in WT and kiBVM mice. Under physiological conditions, PrP^{C} undergoes endoproteolytic cleavage in the vicinity of residues 110/111 to release an N-terminal N1 fragment, leaving behind a membrane-anchored C-terminal fragment termed C1 (Altmeppen et al., 2012). Following the removal of N-linked glycans from PrP using PNGase F, the C1 fragment was observed in brain homogenates from both WT and kiBVM mice (Fig. 1D). Brain BVPrP levels did not change with age in kiBVM mice, and there were no apparent differences in brain BVPrP expression levels between male and female mice (Fig. 1E).

We also examined PrP expression levels in peripheral tissues from WT and kiBVM mice. Using an antibody that does not detect the C1 fragment, comparable levels of PrP expression were found in brain, spinal cord, stomach, spleen, skin, testis, lung, heart, muscle, and tongue tissue between the two mouse lines (Fig. 2A). Varying amounts of diglycosylated, monoglycosylated, and unglycosylated PrP species were observed across the different tissues. Interestingly, an increase in PrP species that migrated more rapidly was found when analyzing testis tissue. This likely corresponds to the C2 endoproteolytic fragment, which results from cleavage of PrP near residue 90. Using an antibody that detects full-length, C1, and C2 PrP species, PrP expression levels in peripheral tissues were found to be much lower than those observed in the brain and spinal cord **(**Fig. 2B**).** Endoproteolytic processing of PrP to produce the C1 fragment was observed in brain, spinal cord, heart, muscle, tongue, and skin tissue, but not in the lungs or testis. Overall, we conclude that kiBVM mice express physiological levels of PrP, both in the central nervous system and in peripheral tissues.

Transgenic mice overexpressing WT BVPrP(I109) spontaneously develop prion disease as they age (Watts et al., 2016; Watts et al., 2012). In contrast, knock-in mice expressing physiological levels of WT BVPrP (I109) remain healthy up to 20 months of age (Mehra et al., 2024). One study reported that transgenic mice overexpressing BVPrP(M109) develop a spontaneous but non-transmissible proteinopathy that lacks biochemical features associated with prion disease such as the presence of protease-resistant PrP in the brain (Kobayashi et al., 2019). Thus, we asked whether aged kiBVM mice develop spontaneous disease. Cohorts of 9–10 kiBVM and WT mice were monitored longitudinally for the

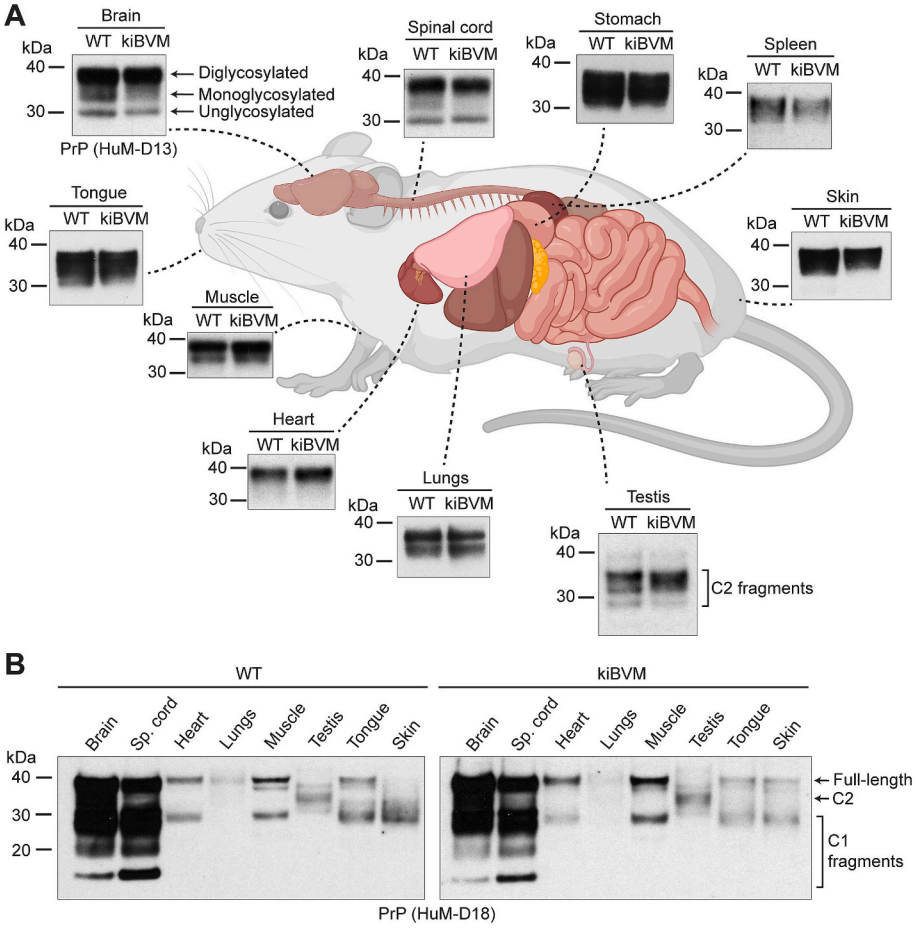

Fig. 2. Tissue expression profile of PrP in wild-type and BVPrP knock-in mice. A) Representative immunoblots for PrP in extracts prepared from brain, spinal cord, stomach, spleen, skin, testis, lung, heart, tongue, and muscle tissue from WT C57BL/6 and kiBVM mice. For the brain tissue immunoblot, di-, mono-, and unglycosylated PrP species are indicated. For the testis immunoblot, putative C2 endoproteolytic products are marked. PrP was detected using the antibody HuM-D13. The mouse organ schematic was generated using BioRender.com. B) Immunoblots for relative PrP expression levels in the indicated tissues from either a WT C57BL/6 mouse (left blot) or a kiBVM mouse (right blot). Full-length PrP as well as the C1 and C2 endoproteolytic fragments are indicated. PrP was detected using the antibody HuM-D18.

development of clinical signs of neurological illness. All kiBVM and WT mice remained free of neurological illness up to 20 months of age (Fig. 3A). As expected, PrP levels in the brain did not differ between WT and kiBVM mice at 20 months of age (Fig. 3B). On average, levels of detergent-insoluble PrP species in brain homogenates from 20-month-old kiBVM mice were approximately 25 % lower than in age-matched brain homogenates from WT mice (Fig. 3C, D). As a positive control, we included brain homogenates from spontaneously ill kiBVI^{D178N} and kiBVI^{E200K} mice that express mutant BVPrP(I109) (Mehra et al., 2024). Despite lower levels of total PrP expression (Fig. 3B), increased amounts of detergent-insoluble PrP were present in the brains of spontaneously sick kiBVI^{D178N} and kiBVI^{E200K} mice compared to asymptomatic 20-month-old WT and kiBVM mice (Fig. 3C). Finally, we looked for the presence of thermolysin (TL)-resistant PrP species in brain homogenates from aged WT and kiBVM mice. Consistent with previous findings (Mehra et al., 2024), TL-resistant PrP could be detected in brain homogenates from spontaneously ill kiBVI^{D178N} and kiBVI^{E200K} mice (Fig. 3E). However, no detergent-insoluble TL-resistant PrP species were observed in the brains of any of the aged WT or kiBVM mice. We therefore conclude that kiBVM mice do not develop spontaneous disease or exhibit misfolded PrP species in their brains with aging.

The interactome of a protein can be considered the complete set of proteins with which that protein interacts. Previously, the interactome of mouse PrP^{C} in brain tissue and cultured cells has been investigated using time-controlled transcardiac perfusion crosslinking (tcTPC) (Ghodrati et al., 2018; Schmitt-Ulms et al., 2004; Watts et al., 2009; Williams et al., 2021). In this technique, proteins residing in close spatial proximity are covalently linked together by perfusing mice with formaldehyde prior to brain removal. Immunoprecipitation is used to isolate PrP^{C}-containing crosslinked protein complexes and then, after reduction, alkylation, and trypsinization, samples are subjected to liquid chromatography followed by tandem mass spectrometry (LC-MS/MS) to identify potential PrP^{C}-interacting proteins (Fig. 4A). To compare the interactomes of BVPrP and MoPrP, 3 kiBVM, 3 WT, and 2 PrP$^{-/-}$ mice at 3 months of age were subjected to tcTPC, their brains were removed and homogenized, and then PrP^{C}-containing complexes were isolated by immunoprecipitation using the HuM-D18 antibody. An immunoblot confirmed the successful immunoprecipitation of crosslinked brain PrP^{C}-containing complexes, which are indicated by the presence of high molecular weight smears in the eluates from WT and kiBVM, but not PrP$^{-/-}$ mice (Fig. 4B).

Following LC-MS/MS, potential PrP^{C}-interacting proteins were identified by applying stringent criteria that required each protein to have been identified by at least 2 unique peptide-to-spectrum matches (PSMs) and that the ratio of the number of PSMs identified in the kiBVM samples to the number of PSMs identified in the PrP$^{-/-}$ samples was greater than 3. Hits were then ranked based on the average number of PSMs in the kiBVM samples minus the average number of PSMs in the PrP$^{-/-}$ samples. The top 30 identified proteins from the brains of kiBVM mice are shown in Fig. 5 and the complete interactome dataset is provided in **Table S1**. Not surprisingly, the top hit in the BVPrP interactome was the prion protein itself, indicating that the targeted pull-down of PrP^{C}-containing complexes was successful. Other confidently identified hits included NCAM1 and NCAM2; the α1, α2, α3, and β1 subunits of

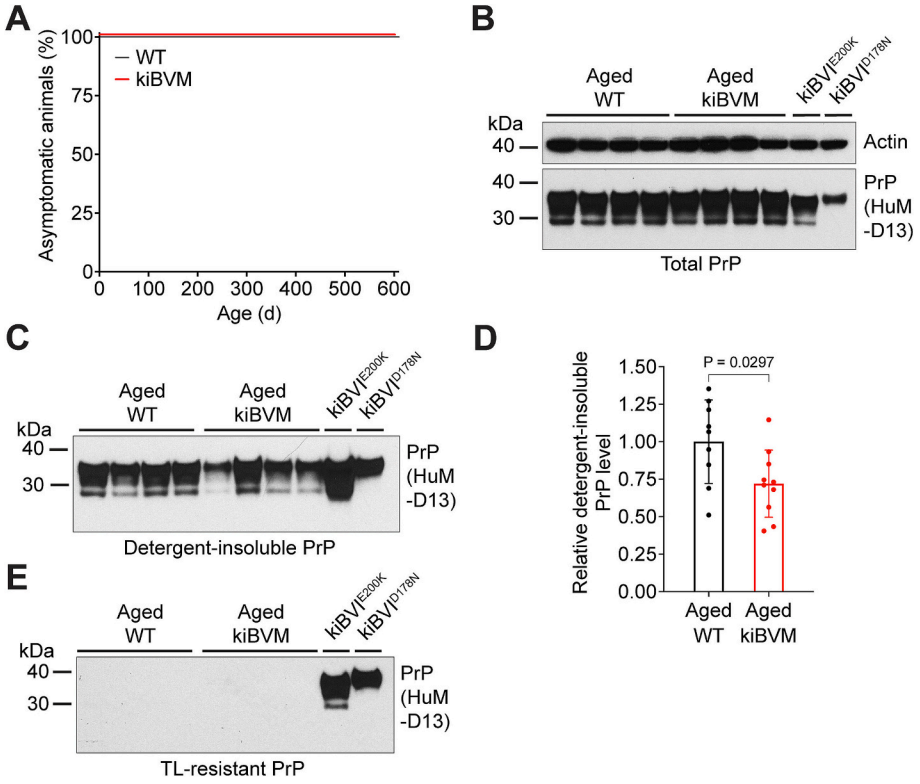

Fig. 3. Knock-in mice expressing BVPrP(M109) do not develop spontaneous disease. A) Kaplan-Meier survival curves for WT C57BL/6 (black line; $n = 9$) and kiBVM (red line; $n = 10$) mice. B) Immunoblot of total PrP levels in detergent-extracted brain homogenates from aged asymptomatic (18- to 20-months-old) WT C57BL/6 and kiBVM mice (n = 4 each). Brain homogenates from spontaneously ill kiBVI^{E200K} and kiBVI^{D178N} mice are also shown. The blot was reprobed with an antibody against actin. C) Immunoblot of detergent-insoluble PrP levels in brain homogenates from aged asymptomatic WT C57BL/6 and kiBVM mice (n = 4 each). Brain homogenates from spontaneously ill kiBVI^{E200K} and kiBVI^{D178N} mice are shown as positive controls. D) Quantification of detergent-insoluble PrP levels in brain homogenates from aged asymptomatic WT C57BL/6 (n = 9) and kiBVM (n = 10) mice. Statistical significance was assessed using a two-tailed Welch's *t*-test. E) Immunoblot for thermolysin (TL)-resistant PrP in brain homogenates from aged asymptomatic WT C57BL/6 and kiBVM mice (n = 4 each). Brain homogenates from spontaneously ill kiBVI^{E200K} and kiBVI^{D178N} mice are shown as positive controls. In panels B, C, and E, PrP was detected using the antibody HuM-D13. (For interpretation of the references to colour in this figure legend, the reader is referred to the web version of this article.)

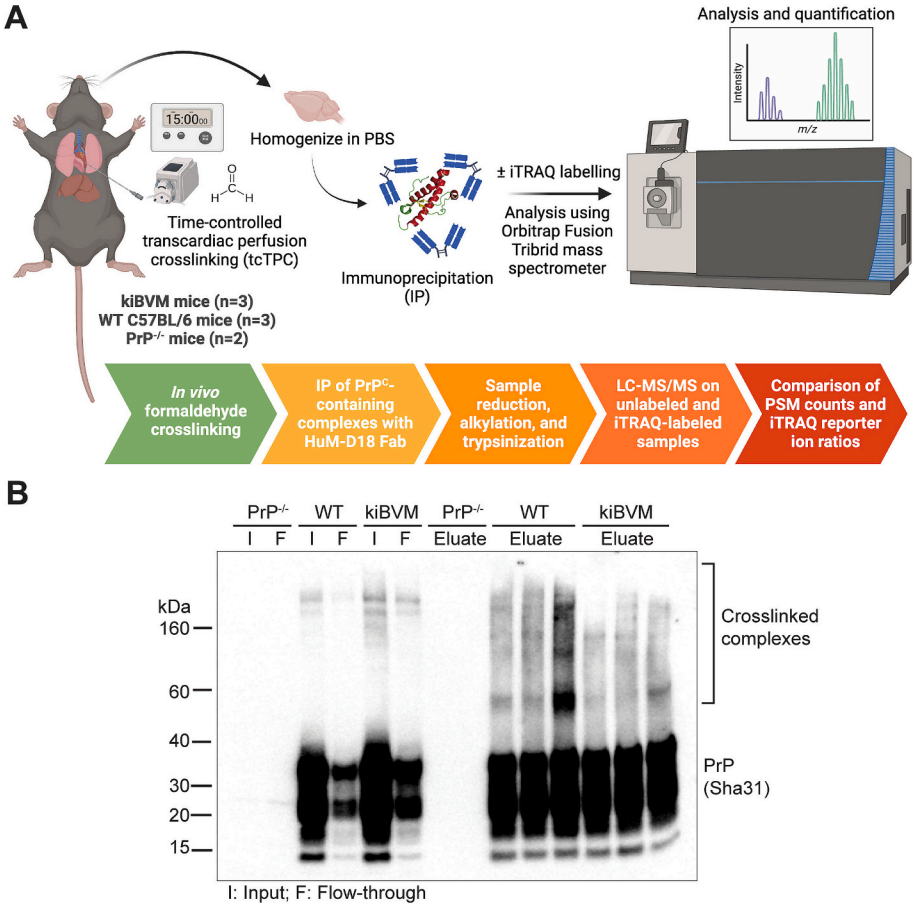

Fig. 4. Workflow for interactome experiments following time-controlled transcardiac perfusion crosslinking in mice. A) Schematic workflow for the mass spectrometry-based comparative PrP^{C} interactome experiments in the brains of kiBVM, WT C57BL/6, and $PrP^{-/-}$ mice. The schematic was generated using BioRender.com. B) Immunoblot for PrP in brain homogenates from $PrP^{-/-}$ mice ($n = 2$), WT C57BL/6 mice ($n = 3$), and kiBVM mice (n = 3) subjected to tcTPC and then immunoprecipitated using the anti-PrP antibody HuM-D18. The fractions shown are the input (I; pre-immunoprecipitation), flow-through (F; non-bound fraction following immunoprecipitation), and eluate (bound fraction following immunoprecipitation). PrP was detected with the Sha31 antibody.

NKAs; DPP6; contactin-1; the protein disulfide isomerase P4HB; and synaptic vesicle glycoprotein 2B (SV2B); all of which have been identified in previous PrP^{C} interactome studies (Ghodrati et al., 2018; Schmitt-Ulms et al., 2004; Watts et al., 2009; Williams et al., 2021). For each of the the top 30 proteins identified in the BVPrP interactome, we also calculated the average number of PSMs identified in samples from WT mice minus the average number of PSMs from the $PrP^{-/-}$ mice. This analysis revealed that 27 of the top 30 BVPrP-interacting proteins were also present in the MoPrP interactome dataset, indicative of substantial overlap between the BVPrP and MoPrP interactomes (Fig. 5). The remaining 3 proteins were also identified but didn't reach the specificity threshold of a WT:$PrP^{-/-}$ PSM ratio of at least 3. We also computed the MoPrP interactome by ranking the identified proteins based on their enrichment in WT mice (**Fig. S1**). Remarkably, 25 of the top 30 proteins identified in the MoPrP interactome were also top 30 hits in the BVPrP interactome, and the other 5 proteins were present in the BVPrP interactome but did not make the top 30.

To determine whether any of the identified proteins may associate more strongly with either BVPrP or MoPrP, we performed quantitative LC-MS/MS analysis on the tcTPC-treated brain samples using isobaric tags for relative and absolute quantitation (iTRAQ) (Ross et al., 2004). In the previous analyses using unlabeled samples, quantitative assessment of individual protein hits was not possible since the mass spectrometry runs on the immunoprecipitated brain samples were conducted independently. Following reduction, alkylation, and trypsin digestion, each of the 8 pull-down samples was labeled with a different 8-plex iTRAQ reagent and then combined and analyzed together by LC-MS/MS. iTRAQ reporter ion ratios relative to one of the two $PrP^{-/-}$ samples were calculated to determine the relative enrichment of specific peptides in the different samples. The complete iTRAQ-labeled dataset is shown in **Table S2**. Peptides corresponding to PrP were strongly enriched in all the pull-down samples from the brains of both kiBVM and WT mice, but not in the sample from the other $PrP^{-/-}$ brain (Fig. 6A, top panel). When only peptides containing at least one of the eight BVPrP-specific residues (i.e., not present in the MoPrP sequence) were considered, iTRAQ reporter ion enrichment was only observed for the samples from kiBVM mice (Fig. 6A, lower panel). Conversely, when only peptides containing at least one MoPrP-specific residue (i.e., not present in the BVPrP sequence) were analyzed, enrichment was only observed in the samples from WT mice (**Fig. S2**). A non-specific interactor such as glyceraldehyde-3-phosphate dehydrogenase (GAPDH), which likely associates with the immunoprecipitation matrix, did not exhibit any consistent iTRAQ reporter ion enrichment across the kiBVM, WT, and $PrP^{-/-}$ samples (**Fig. S3**). iTRAQ reporter ion ratios for the top putative PrP^{C}-interacting proteins were compared between the kiBVM and WT samples. Although there was considerable variability between samples, there were no significant differences in the relative enrichments between kiBVM and WT mice for any of the proteins (Fig. 6B). Thus, the quantitative iTRAQ labelling data is consistent with the unlabeled experiments where PSM counts were compared, with both sets of experiments suggesting that the interactomes of BVPrP and MoPrP in healthy mice are highly congruent.

				BVPrP interactome											MoPrP interactome	
Rank in BVPrP interactome	Accession	Description (curated)	Gene	Coverage	Unique peptides	Total peptides	# PSM kiBVM (1)	# PSM kiBVM (2)	# PSM kiBVM (3)	# PSM KO (1)	# PSM KO (2)	Avg PSM kiBVM	Avg PSM KO	Avg PSM kiBVM minus Avg PSM KO	Avg PSM WT minus Avg PSM KO	Rank in MoPrP interactome
1	Q8VHV5	Major prion protein	Prnp	87.90%	5	18	190	198	236			208.00	0.00	208.00	182.67	1
2	Q6PIC6	Sodium/potassium-transporting ATPase subunit alpha-3	Atp1a3	64.66%	33	67	204	248	265	50	51	239.00	50.50	188.50	131.50	2
3	E9QB01	Neural cell adhesion molecule 1	Ncam1	70.08%	6	45	107	147	161		6	138.33	3.00	135.33	92.33	3
4	Q8VDN2	Sodium/potassium-transporting ATPase subunit alpha-1	Atp1a1	52.39%	22	59	145	168	159	44	32	157.33	38.00	119.33	81.67	4
5	Q6PIE5	Sodium/potassium-transporting ATPase subunit alpha-2	Atp1a2	57.45%	25	71	147	173	139	37	35	153.00	36.00	117.00	76.67	5
6	P12960	Contactin-1	Cntn1	62.25%	35	57	56	90	89	6	8	78.33	7.00	71.33	48.00	6
7	Q8BG39	Synaptic vesicle glycoprotein 2B	Sv2b	44.36%	13	26	61	49	58	8	3	56.00	5.50	50.50	39.17	7
8	P14094	Sodium/potassium-transporting ATPase subunit beta-1	Atp1b1	61.51%	10	16	36	52	57	5	8	48.33	6.50	41.83	22.50	12
9	A2AFG8	Neural cell adhesion molecule L1	L1cam	58.25%	16	48	38	47	61	7	12	48.67	9.50	39.17	28.83	8
10	P63101	14-3-3 protein zeta/delta	Ywhaz	88.16%	12	24	34	47	48	10	5	43.00	7.50	35.50	19.17	15
11	Q5U4C2	Dipeptidyl aminopeptidase-like protein 6	Dpp6	64.17%	18	41	23	39	37			33.00	0.00	33.00	21.33	13
12	Q810U4-2	Isoform 2 of Neuronal cell adhesion molecule	Nrcam	56.24%	16	54	23	34	55	8	5	37.33	6.50	30.83	12.50	23
13	Q04447	Creatine kinase B-type	Ckb	84.51%	15	24	42	42	52	18	11	45.33	14.50	30.83	20.17*	
14	O35136	Neural cell adhesion molecule 2	Ncam2	55.44%	19	47	28	35	38	6		33.67	3.00	30.67	22.67	11
15	P61264	Syntaxin-1B	Stx1b	61.46%	11	21	37	32	31	6		33.33	3.00	30.33	20.00	14
16	P46096	Synaptotagmin-1	Syt1	48.69%	10	22	29	34	27			30.00	0.00	30.00	22.67	10
17	P62874	Guanine nucleotide-binding protein G(I)/G(S)/G(T) subunit beta-1	Gnb1	77.65%	5	20	31	34	35	6	5	33.33	5.50	27.83	18.50	16
18	P17183	Gamma-enolase	Eno2	79.95%	15	27	30	30	42	11	7	34.00	9.00	25.00	14.33*	
19	P60879	Synaptosomal-associated protein 25	Snap25	77.67%	2	18	25	24	24			24.33	0.00	24.33	27.00	9
20	E9Q3Q6	CD166 antigen	Alcam	71.23%	12	38	20	34	24		5	26.00	2.50	23.50	11.83	26
21	Q02053	Ubiquitin-like modifier-activating enzyme 1	Uba1	57.28%	14	42	21	42	25	5	8	29.33	6.50	22.83	14.17	18
22	E9QKR0	Guanine nucleotide-binding protein G(I)/G(S)/G(T) subunit beta-2	Gnb2	60.47%	2	16	16	24	28			22.67	0.00	22.67	17.00	17
23	P09103	Protein disulfide-isomerase	P4hb	55.80%	16	24	25	18	23			22.00	0.00	22.00	13.00	20
24	P56564	Excitatory amino acid transporter 1	Slc1a3	34.62%	6	15	28	26	24	4	5	26.00	4.50	21.50	11.50	28
25	Q9JIS5	Synaptic vesicle glycoprotein 2A	Sv2a	43.40%	8	22	31	18	35	7	6	28.00	6.50	21.50	12.83	22
26	P12023	Amyloid beta A4 protein	App	57.14%	11	29	18	19	25			20.67	0.00	20.67	10.00	38
27	O35526	Syntaxin-1A	Stx1a	59.72%	5	17	24	16	19			19.67	0.00	19.67	11.33	29
28	P17742	Peptidyl-prolyl cis-trans isomerase A	Ppia	73.78%	10	14	18	25	30	7	7	24.33	7.00	17.33	7.33*	
29	P46097	Synaptotagmin-2	Syt2	45.02%	3	17	17	19	15			17.00	0.00	17.00	11.33	30
30	Q3UHL1	CaM kinase-like vesicle-associated protein	Camkv	67.58%	12	27	18	29	19	7	3	22.00	5.00	17.00	10.67	36

Fig. 5. The brain interactome of bank vole PrP. Top 30 identified BVPrP-interacting proteins ranked by the average number of peptide-to-spectrum matches (PSMs) observed in kiBVM mice (n = 3) minus the average number of PSMs observed in $PrP^{-/-}$ mice (KO; n = 2). For each protein identified, the average number of PSMs observed in WT mice (n = 3) minus the average number of PSMs from $PrP^{-/-}$ mice as well as the rank in the MoPrP interactome are also shown. Coverage, represented by grey shading, indicates the percentage of primary structure covered by PSMs across the three kiBVM samples. Blue-shaded numbers reflect the number of PSMs detected and green-shaded numbers reflect the relative enrichment in kiBVM or WT versus $PrP^{-/-}$ samples. Orange shading with an asterisk indicates those proteins that were also found in the MoPrP interactome but didn't reach the specificity threshold (WT:KO PSM ratio of at least 3). (For interpretation of the references to colour in this figure legend, the reader is referred to the web version of this article.)

4. Discussion

Transgenic mice expressing BVPrP retain the ability of bank voles to function as a universal prion acceptor, suggesting that the primary sequence of BVPrP is the main driver of its prion permissive behavior (Espinosa et al., 2016; Watts et al., 2014). Additionally, this suggests that if altered protein-protein interactions, mediated by BVPrP-specific residues, are responsible for facilitating cross-species prion replication, these interactions must be conserved when BVPrP is expressed in mice. In this study, we compared the interactomes of MoPrP and BVPrP in mice to discern any novel protein-protein interactions that could explain the heightened susceptibility of bank voles to prions. To avoid potential artifacts associated with PrP^{C} overexpression in transgenic mice, we generated knock-in mice that express BVPrP(M109) at physiological levels under the control of the endogenous mouse *Prnp* promoter. This ensured that MoPrP and BVPrP were expressed at the same levels in the brains of mice and with the same spatiotemporal pattern of expression. Although we have not yet confirmed that kiBVM mice are susceptible to a diverse array of prion strains, it has been shown that a distinct line of knock-in mice expressing BVPrP(M109) can be readily infected with several different strains of human prions (Kobayashi et al., 2019). We found that the interactomes of MoPrP and BVPrP were remarkably similar, with no unique interactors identified for either protein. This suggests that the molecular environments of MoPrP and BVPrP within the plasma membrane of brain cells are highly similar, if not identical. We note that there was sample-to-sample variability in both the unlabeled and iTRAQ-labeled datasets, which may have obscured more subtle differences in protein-protein interactions involving MoPrP or BVPrP. There was a general trend where average PSM counts and iTRAQ reporter ion ratios for PrP-interacting proteins were higher in samples from kiBVM than WT mice (**Table S1, Table S2**). This was largely driven by lower signals in the 2nd and 3rd WT samples, which could potentially be explained by a lower crosslinking efficiency in these mice.

Although it has been firmly established that BVPrP(I109) is prone to spontaneous misfolding (Erana et al., 2023; Fernandez-Borges et al., 2018; Mehra et al., 2024; Otero et al., 2019; Watts et al., 2016; Watts et al., 2012), it is less clear whether BVPrP(M109) can also form prions spontaneously. In one study, transgenic mice overexpressing BVPrP (M109) developed clinical disease, but without accompanying biochemical features characteristic of prion disease, such as the presence of protease-resistant PrP (Kobayashi et al., 2019). No disease transmission was observed upon inoculation of brain extracts from spontaneously sick BVPrP(M109) transgenic mice into knock-in mice expressing BVPrP(M109), suggesting that overexpression of BVPrP (M109) causes a PrP proteinopathy without spontaneous prion formation. We found that, like WT mice expressing MoPrP, kiBVM mice remained healthy throughout their normal lifespans without any evidence for an increase in misfolded BVPrP species in the brains of aged mice. This is identical to what we observed in knock-in mice expressing the more misfolding-prone BVPrP(I109) (Mehra et al., 2024), arguing that BVPrP overexpression is required to elicit spontaneous disease and prion generation, which is consistent with absence of reported spontaneous prion disease in bank voles.

The issue of whether proteins other than PrP participate in prion formation or replication remains an unsolved mystery (Eid et al., 2024). Given its prion permissive nature, we speculated that BVPrP may represent an ideal means for identifying such proteins. However, both our unlabeled and iTRAQ-labeled interactome datasets failed to reveal proteins that selectively interact with BVPrP. Moreover, since we also did not detect any proteins that selectively interact with MoPrP, this makes a scenario where the enhanced prion replication properties of BVPrP stem from a reduced ability to interact with a negative regulator of prion replication less plausible. Nonetheless, our interactome studies did reveal that BVPrP interacts with many previously identified MoPrP interactors. A top hit for both BVPrP and MoPrP was NCAM1, which has been robustly identified as a PrP^{C}-interacting protein in several lines of cultured cells and in mice (Ghodrati et al., 2018; Schmitt-Ulms et al., 2004; Schmitt-Ulms et al., 2001; Watts et al., 2009). NCAM1 is unlikely to be involved in prion replication since NCAM1 knockout mice are as susceptible to prions as WT mice (Schmitt-Ulms et al., 2001). In contrast, the interaction between NCAM1 and PrP^{C}, mediated by the flexible N-terminal domain of PrP^{C} and the fibronectin type-3 domain of NCAM, has been shown to promote neurite outgrowth and neuronal differentiation (Prodromidou et al., 2014; Santuccione et al., 2005; Slapsak

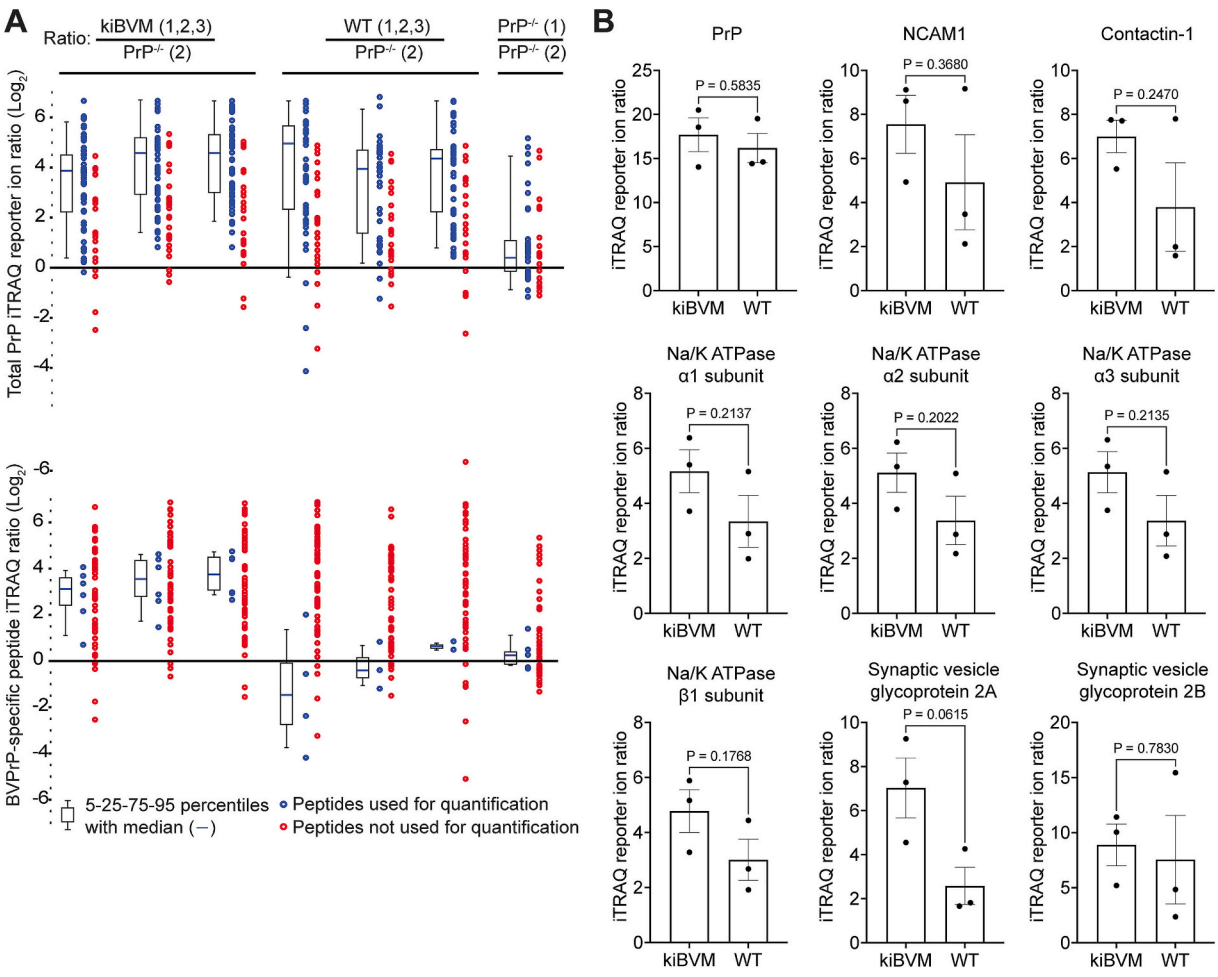

Fig. 6. Quantitative analysis of mouse and bank vole PrP interactors using iTRAQ labeling. A) Boxplots depicting iTRAQ reporter ion enrichment ratios (Log_2) for PrP peptides in immunoprecipitated samples from the brains of kiBVM and WT C57BL/6 mice (n = 3 each) as well as the brain of a $PrP^{-/-}$ mouse. For each sample, the enrichment ratio was calculated in comparison to the second $PrP^{-/-}$ sample. The upper graph displays enrichment ratios for all PrP peptides, whereas the bottom panel displays enrichment ratios for PrP peptides containing at least one of the eight BVPrP-specific amino acids. Peptides that were not used for quantification include those that did not pass the Percolator threshold and those that were excluded to prevent double counting when assigned correctly by both the Sequest and Mascot algorithms in Proteome Discoverer. B) iTRAQ reporter ion ratios (Log_2), all in comparison to the second $PrP^{-/-}$ sample, for a subset of proteins identified in the kiBVM and WT interactome datasets (n = 3 each). Statistical significance was assessed using two-tailed Welch's *t*-tests.

et al., 2016). PrP^C also controls the polysialylation of NCAM1 in cultured cells, a phenomenon that is important for epithelial-to-mesenchymal transition during cellular development (Mehrabian et al., 2015). Another robust hit for both BVPrP and MoPrP were subunits of NKAs, the pumps that are responsible for maintaining the resting potential across the plasma membrane in neural cells. PrP^C co-localizes with the NKA α1 subunit in neural cells and promotes NKA-mediated ion uptake activity in neuronal and astroglial cultures (Kleene et al., 2007; Williams et al., 2021). Subunits of NKAs have also been found in preparations of scrapie-associated fibrils isolated from brains of prion-infected mice (Graham et al., 2011). Interestingly, targeting the NKA α1 subunit with cardiac glycosides results in their internalization as well as the co-internalization and degradation of PrP^C (Mehrabian et al., 2022). Thus, reducing PrP^C levels by targeting the NKA α subunit is a potential strategy for dampening prion replication during prion disease (Eid et al., 2022).

The complexity of the lipid bilayer within which PrP^C resides complicates the identification of PrP^C binding partners. Our experiments, which relied on the mild crosslinking of PrP^C to its nearest neighbors, revealed proteins that are found in the vicinity of PrP^C, and parallel analyses in $PrP^{-/-}$ mice were useful for delineating specific from non-specific interactions. However, because crosslinking was used, it is possible that not all identified proteins physically interact with PrP^C and may simply reside in close spatial proximity within the membrane. Also, our study does not discriminate between direct and indirect interactors of PrP^C, and it is likely that the crosslinking followed by immunoprecipitation approach may not have captured all biologically meaningful protein-protein interactions involving PrP^C. Another limitation of our study is that we only investigated the PrP^C interactome in healthy mice. It remains possible that BVPrP may participate in unique interactions with other proteins that only occur during the conversion of PrP^C into PrP^{Sc}, thus facilitating cross-species prion infection. Furthermore, we only examined protein-protein interactions whereas PrP is known to interact with other types of macromolecules, such as lipids, nucleic acids, and glycosaminoglycans (Callender et al., 2020; Deleault et al., 2003; Lima et al., 2006; Sanghera and Pinheiro, 2002). It is conceivable that BVPrP may exhibit enhanced binding to a non-proteinaceous cofactor that facilitates the conversion of PrP^C into PrP^{Sc}. Indeed, lipid cofactors such as phosphatidylethanolamine have been shown to enhance the templated or spontaneous conversion of mouse PrP^C into PrP^{Sc} in vitro and modulate prion strain properties (Deleault et al., 2012a; Deleault et al., 2012b). Moreover, the presence of phosphatidylethanolamine cofactor was necessary to generate infectious forms of recombinant BVPrP (Burke et al., 2019).

The lack of proteins that bind specifically to BVPrP when expressed in mice is perhaps not surprising, as the structure of the C-terminal

globular domain BVPrP^{C} is very similar to that of PrPs from other species and does not contain unique structural motifs that could mediate novel interactions and facilitate prion replication (Christen et al., 2008). Unlike MoPrP, BVPrP contains a rigid loop in the β2-α2 region, but this microstructure is also present in PrPs from other species such as elk and horses, the latter of which are considered to be quite resistant to prion infection (Gossert et al., 2005; Perez et al., 2010). Notably, recombinant BVPrP behaves as a universal substrate for the detection of prion seeds in the real-time quaking-induced conversion assay and spontaneously polymerizes into aggregates much faster than PrPs from other species (Arshad et al., 2024; Orru et al., 2015). Therefore, independent of other proteins or cofactors, BVPrP is inherently prone to adopting misfolded conformations. Thus, when paired with our interactome data, the anomalous properties of BVPrP are more likely to be rooted in its intrinsic thermodynamic properties rather than the existence of unique protein-protein interactions.

Funding

This work was funded by grants from the Canadian Institutes of Health Research (#PJT-169048) and the Natural Sciences and Engineering Research Council (NSERC) of Canada (#RGPIN-2015-05112) to JCW. SM was supported by a fellowship from the CJD Foundation. The funding bodies had no role in the design of the study, the collection, analysis, or interpretation of data, or the writing of the manuscript.

CRediT authorship contribution statement

Hamza Arshad: Writing – review & editing, Writing – original draft, Visualization, Investigation, Formal analysis, Data curation, Conceptualization. **Shehab Eid:** Writing – review & editing, Investigation. **Surabhi Mehra:** Writing – review & editing, Investigation. **Declan Williams:** Writing – review & editing, Methodology, Investigation, Data curation. **Lech Kaczmarczyk:** Writing – review & editing, Resources, Investigation. **Erica Stuart:** Writing – review & editing, Investigation. **Walker S. Jackson:** Writing – review & editing, Resources, Conceptualization. **Gerold Schmitt-Ulms:** Writing – review & editing, Supervision, Methodology, Formal analysis, Conceptualization. **Joel C. Watts:** Writing – review & editing, Writing – original draft, Visualization, Supervision, Funding acquisition, Formal analysis, Conceptualization.

Declaration of competing interest

The authors declare the following financial interests/personal relationships which may be considered as potential competing interests:

Joel C. Watts reports financial support was provided by Canadian Institutes of Health Research. Joel C. Watts reports financial support was provided by Natural Sciences and Engineering Research Council of Canada. Surabhi Mehra reports financial support was provided by CJD Foundation. If there are other authors, they declare that they have no known competing financial interests or personal relationships that could have appeared to influence the work reported in this paper.

Acknowledgements

The authors thank Rosemary Ahrens for assistance with the mouse perfusions and Stanley Prusiner (University of California San Francisco) for providing the HuM-D13 and HuM-R1 antibodies. Experimental schematics were created using BioRender.com.

Appendix A. Supplementary data

Supplementary data to this article can be found online at https://doi.org/10.1016/j.nbd.2025.106802.

Data availability

The mass spectrometry proteomics data have been deposited to the ProteomeXchange Consortium via the PRIDE partner repository with the dataset identifier PXD059662. All other data generated or analyzed during this study are included in this published article.

References

Agrimi, U., Nonno, R., Dell'Omo, G., et al., 2008. Prion protein amino acid determinants of differential susceptibility and molecular feature of prion strains in mice and voles. PLoS Pathog. 4, e1000113. https://doi.org/10.1371/journal.ppat.1000113.

Altmeppen, H.C., Puig, B., Dohler, F., et al., 2012. Proteolytic processing of the prion protein in health and disease. Am. J. Neurodegener. Dis. 1, 15–31.

Arshad, H., Bourkas, M.E.C., Watts, J.C., 2020. The utility of bank voles for studying prion disease. Prog. Mol. Biol. Transl. Sci. 175, 179–211. https://doi.org/10.1016/bs.pmbts.2020.08.009.

Arshad, H., Patel, Z., Amano, G., et al., 2023. A single protective polymorphism in the prion protein blocks cross-species prion replication in cultured cells. J. Neurochem. 165, 230–245. https://doi.org/10.1111/jnc.15739.

Arshad, H., Patel, Z., Al-Azzawi, Z.A.M., et al., 2024. The molecular determinants of a universal prion acceptor. PLoS Pathog. 20, e1012538. https://doi.org/10.1371/journal.ppat.1012538.

Brandner, S., Isenmann, S., Raeber, A., et al., 1996a. Normal host prion protein necessary for scrapie-induced neurotoxicity. Nature 379, 339–343. https://doi.org/10.1038/379339a0.

Brandner, S., Raeber, A., Sailer, A., et al., 1996b. Normal host prion protein (PrPC) is required for scrapie spread within the central nervous system. Proc. Natl. Acad. Sci. USA 93, 13148–13151. https://doi.org/10.1073/pnas.93.23.13148.

Bueler, H., Fischer, M., Lang, Y., et al., 1992. Normal development and behaviour of mice lacking the neuronal cell-surface PrP protein. Nature 356, 577–582. https://doi.org/10.1038/356577a0.

Bueler, H., Aguzzi, A., Sailer, A., et al., 1993. Mice devoid of PrP are resistant to scrapie. Cell 73, 1339–1347. https://doi.org/10.1016/0092-8674(93)90360-3.

Burke, C.M., Walsh, D.J., Steele, A.D., et al., 2019. Full restoration of specific infectivity and strain properties from pure mammalian prion protein. PLoS Pathog. 15, e1007662. https://doi.org/10.1371/journal.ppat.1007662.

Burke, C.M., Mark, K.M.K., Walsh, D.J., et al., 2020. Identification of a homology-independent linchpin domain controlling mouse and bank vole prion protein conversion. PLoS Pathog. 16, e1008875. https://doi.org/10.1371/journal.ppat.1008875.

Callender, J.A., Sevillano, A.M., Soldau, K., et al., 2020. Prion protein post-translational modifications modulate heparan sulfate binding and limit aggregate size in prion disease. Neurobiol. Dis. 142, 104955. https://doi.org/10.1016/j.nbd.2020.104955.

Cartoni, C., Schinina, M.E., Maras, B., et al., 2005. Identification of the pathological prion protein allotypes in scrapie-infected heterozygous bank voles (*Clethrionomys glareolus*) by high-performance liquid chromatography-mass spectrometry. J. Chromatogr. A 1081, 122–126. https://doi.org/10.1016/j.chroma.2005.04.035.

Christen, B., Perez, D.R., Hornemann, S., Wuthrich, K., 2008. NMR structure of the bank vole prion protein at 20 degrees C contains a structured loop of residues 165-171. J. Mol. Biol. 383, 306–312. https://doi.org/10.1016/j.jmb.2008.08.045.

Ciric, D., Richard, C.A., Moudjou, M., et al., 2015. Interaction between Shadoo and PrP affects the PrP-folding pathway. J. Virol. 89, 6287–6293. https://doi.org/10.1128/JVI.03429-14.

Colby, D.W., Prusiner, S.B., 2011. Prions. Cold Spring Harb. Perspect. Biol. 3, a006833. https://doi.org/10.1101/cshperspect.a006833.

Collinge, J., Clarke, A.R., 2007. A general model of prion strains and their pathogenicity. Science 318, 930–936. https://doi.org/10.1126/science.1138718.

Cosseddu, G.M., Nonno, R., Vaccari, G., et al., 2011. Ultra-efficient PrP(Sc) amplification highlights potentialities and pitfalls of PMCA technology. PLoS Pathog. 7, e1002370. https://doi.org/10.1371/journal.ppat.1002370.

Daude, N., Wohlgemuth, S., Brown, R., et al., 2012. Knockout of the prion protein (PrP)-like Sprn gene does not produce embryonic lethality in combination with PrP(C)-deficiency. Proc. Natl. Acad. Sci. USA 109, 9035–9040. https://doi.org/10.1073/pnas.1202130109.

Deleault, N.R., Lucassen, R.W., Supattapone, S., 2003. RNA molecules stimulate prion protein conversion. Nature 425, 717–720. https://doi.org/10.1038/nature01979.

Deleault, N.R., Piro, J.R., Walsh, D.J., et al., 2012a. Isolation of phosphatidylethanolamine as a solitary cofactor for prion formation in the absence of nucleic acids. Proc. Natl. Acad. Sci. USA 109, 8546–8551. https://doi.org/10.1073/pnas.1204498109.

Deleault, N.R., Walsh, D.J., Piro, J.R., et al., 2012b. Cofactor molecules maintain infectious conformation and restrict strain properties in purified prions. Proc. Natl. Acad. Sci. USA 109, E1938–E1946. https://doi.org/10.1073/pnas.1206999109.

Di Bari, M.A., Nonno, R., Castilla, J., et al., 2013. Chronic wasting disease in bank voles: characterisation of the shortest incubation time model for prion diseases. PLoS Pathog. 9, e1003219. https://doi.org/10.1371/journal.ppat.1003219.

Eid, S., Zerbes, T., Williams, D., et al., 2022. Identification of a cardiac glycoside exhibiting favorable brain bioavailability and potency for reducing levels of the cellular prion protein. Int. J. Mol. Sci. 23, 14823. https://doi.org/10.3390/ijms232314823.

Eid, S., Lee, S., Verkuyl, C.E., et al., 2024. The importance of prion research. Biochem. Cell Biol. https://doi.org/10.1139/bcb-2024-0018.

Erana, H., Charco, J.M., Di Bari, M.A., et al., 2019. Development of a new largely scalable in vitro prion propagation method for the production of infectious recombinant prions for high resolution structural studies. PLoS Pathog. 15, e1008117. https://doi.org/10.1371/journal.ppat.1008117.

Erana, H., Diaz-Dominguez, C.M., Charco, J.M., et al., 2023. Understanding the key features of the spontaneous formation of bona fide prions through a novel methodology that enables their swift and consistent generation. Acta Neuropathol. Commun. 11, 145. https://doi.org/10.1186/s40478-023-01640-8.

Espinosa, J.C., Nonno, R., Di Bari, M., et al., 2016. PrPC governs susceptibility to prion strains in Bank vole, while other host factors modulate strain features. J. Virol. 90, 10660–10669. https://doi.org/10.1128/JVI.01592-16.

Fang, C., Imberdis, T., Garza, M.C., Wille, H., Harris, D.A., 2016. A neuronal culture system to detect prion synaptotoxicity. PLoS Pathog. 12, e1005623. https://doi.org/10.1371/journal.ppat.1005623.

Fernandez-Borges, N., Di Bari, M.A., Erana, H., et al., 2018. Cofactors influence the biological properties of infectious recombinant prions. Acta Neuropathol. 135, 179–199. https://doi.org/10.1007/s00401-017-1782-y.

Ghodrati, F., Mehrabian, M., Williams, D., et al., 2018. The prion protein is embedded in a molecular environment that modulates transforming growth factor beta and integrin signaling. Sci. Rep. 8, 8654. https://doi.org/10.1038/s41598-018-26685-x.

Gossert, A.D., Bonjour, S., Lysek, D.A., Fiorito, F., Wuthrich, K., 2005. Prion protein NMR structures of elk and of mouse/elk hybrids. Proc. Natl. Acad. Sci. USA 102, 646–650. https://doi.org/10.1073/pnas.0409008102.

Graham, J.F., Kurian, D., Agarwal, S., et al., 2011. Na+/K+-ATPase is present in scrapie-associated fibrils, modulates PrP misfolding in vitro and links PrP function and dysfunction. PLoS One 6, e26813. https://doi.org/10.1371/journal.pone.0026813.

Han, J., Song, Q.Q., Sun, P., et al., 2014. Interaction between 14-3-3beta and PrP influences the dimerization of 14-3-3 and fibrillization of PrP106-126. Int. J. Biochem. Cell Biol. 47, 20–28. https://doi.org/10.1016/j.biocel.2013.10.013.

Kaczmarczyk, L., Mende, Y., Zevnik, B., Jackson, W.S., 2016. Manipulating the prion protein gene sequence and expression levels with CRISPR/Cas9. PLoS One 11, e0154604. https://doi.org/10.1371/journal.pone.0154604.

Kaneko, K., Zulianello, L., Scott, M., et al., 1997. Evidence for protein X binding to a discontinuous epitope on the cellular prion protein during scrapie prion propagation. Proc. Natl. Acad. Sci. USA 94, 10069–10074. https://doi.org/10.1073/pnas.94.19.10069.

Kleene, R., Loers, G., Langer, J., Frobert, Y., Buck, F., Schachner, M., 2007. Prion protein regulates glutamate-dependent lactate transport of astrocytes. J. Neurosci. 27, 12331–12340. https://doi.org/10.1523/JNEUROSCI.1358-07.2007.

Kobayashi, A., Matsuura, Y., Takeuchi, A., et al., 2019. A domain responsible for spontaneous conversion of bank vole prion protein. Brain Pathol. 29, 155–163. https://doi.org/10.1111/bpa.12638.

Kraus, A., Hoyt, F., Schwartz, C.L., et al., 2021. High-resolution structure and strain comparison of infectious mammalian prions. Mol. Cell 81. https://doi.org/10.1016/j.molcel.2021.08.011, 4540–4551 e6.

Kuffer, A., Lakkaraju, A.K., Mogha, A., et al., 2016. The prion protein is an agonistic ligand of the G protein-coupled receptor Adgrg6. Nature 536, 464–468. https://doi.org/10.1038/nature19312.

Lima, L.M.T.R., Cordeiro, Y., Tinoco, L.W., et al., 2006. Structural insights into the interaction between prion protein and nucleic acid. Biochemistry 45, 9180–9187. https://doi.org/10.1021/bi060532d.

Manka, S.W., Zhang, W., Wenborn, A., et al., 2022. 2.7 A cryo-EM structure of ex vivo RML prion fibrils. Nat. Commun. 13, 4004. https://doi.org/10.1038/s41467-022-30457-7.

McKinley, M.P., Bolton, D.C., Prusiner, S.B., 1983. A protease-resistant protein is a structural component of the scrapie prion. Cell 35, 57–62. https://doi.org/10.1016/0092-8674(83)90207-6.

Mehra, S., Bourkas, M.E., Kaczmarczyk, L., et al., 2024. Convergent generation of atypical prions in knockin mouse models of genetic prion disease. J. Clin. Invest. 134, e176344. https://doi.org/10.1172/JCI176344.

Mehrabian, M., Brethour, D., Wang, H., Xi, Z., Rogaeva, E., Schmitt-Ulms, G., 2015. The prion protein controls Polysialylation of neural cell adhesion molecule 1 during cellular morphogenesis. PLoS One 10, e0133741. https://doi.org/10.1371/journal.pone.0133741.

Mehrabian, M., Wang, X., Eid, S., et al., 2022. Cardiac glycoside-mediated turnover of Na, K-ATPases as a rational approach to reducing cell surface levels of the cellular prion protein. PLoS One 17, e0270915. https://doi.org/10.1371/journal.pone.0270915.

Mercer, R.C., Ma, L., Watts, J.C., et al., 2013. The prion protein modulates A-type K+ currents mediated by Kv4.2 complexes through dipeptidyl aminopeptidase-like protein 6. J. Biol. Chem. 288, 37241–37255. https://doi.org/10.1074/jbc.M113.488650.

Mok, T.H., Nihat, A., Luk, C., et al., 2021. Bank vole prion protein extends the use of RT-QuIC assays to detect prions in a range of inherited prion diseases. Sci. Rep. 11, 5231. https://doi.org/10.1038/s41598-021-84527-9.

Nonno, R., Di Bari, M.A., Cardone, F., et al., 2006. Efficient transmission and characterization of Creutzfeldt-Jakob disease strains in bank voles. PLoS Pathog. 2, e12. https://doi.org/10.1371/journal.ppat.0020012.

Nonno, R., Notari, S., Di Bari, M.A., et al., 2019. Variable protease-sensitive Prionopathy transmission to Bank voles. Emerg. Infect. Dis. 25, 73–81. https://doi.org/10.3201/eid2501.180807.

Nonno, R., Di Bari, M.A., Pirisinu, L., et al., 2020. Studies in bank voles reveal strain differences between chronic wasting disease prions from Norway and North America. Proc. Natl. Acad. Sci. USA 117, 31417–31426. https://doi.org/10.1073/pnas.2013237117.

Nuvolone, M., Hermann, M., Sorce, S., et al., 2016. Strictly co-isogenic C57BL/6J-Prnp−/− mice: a rigorous resource for prion science. J. Exp. Med. 213, 313–327. https://doi.org/10.1084/jem.20151610.

Orru, C.D., Groveman, B.R., Raymond, L.D., et al., 2015. Bank vole prion protein as an apparently universal substrate for RT-QuIC-based detection and discrimination of prion strains. PLoS Pathog. 11, e1004983. https://doi.org/10.1371/journal.ppat.1004983.

Otero, A., Hedman, C., Fernandez-Borges, N., et al., 2019. A single amino acid substitution, found in mammals with low susceptibility to prion diseases, delays propagation of two prion strains in highly susceptible transgenic mouse models. Mol. Neurobiol. 56, 6501–6511. https://doi.org/10.1007/s12035-019-1535-0.

Perez, D.R., Damberger, F.F., Wuthrich, K., 2010. Horse prion protein NMR structure and comparisons with related variants of the mouse prion protein. J. Mol. Biol. 400, 121–128. https://doi.org/10.1016/j.jmb.2010.04.066.

Pirisinu, L., Di Bari, M.A., D'Agostino, C., et al., 2016. Gerstmann-Straussler-Scheinker disease subtypes efficiently transmit in bank voles as genuine prion diseases. Sci. Rep. 6, 20443. https://doi.org/10.1038/srep20443.

Pirisinu, L., Di Bari, M.A., D'Agostino, C., et al., 2022. A single amino acid residue in bank vole prion protein drives permissiveness to Nor98/atypical scrapie and the emergence of multiple strain variants. PLoS Pathog. 18, e1010646. https://doi.org/10.1371/journal.ppat.1010646.

Polymenidou, M., Moos, R., Scott, M., et al., 2008. The POM monoclonals: a comprehensive set of antibodies to non-overlapping prion protein epitopes. PLoS One 3, e3872. https://doi.org/10.1371/journal.pone.0003872.

Prodromidou, K., Papastefanaki, F., Sklaviadis, T., Matsas, R., 2014. Functional cross-talk between the cellular prion protein and the neural cell adhesion molecule is critical for neuronal differentiation of neural stem/precursor cells. Stem Cells 32, 1674–1687. https://doi.org/10.1002/stem.1663.

Prusiner, S.B., Scott, M., Foster, D., et al., 1990. Transgenetic studies implicate interactions between homologous PrP isoforms in scrapie prion replication. Cell 63, 673–686. https://doi.org/10.1016/0092-8674(90)90134-z.

Rieger, R., Edenhofer, F., Lasmezas, C.I., Weiss, S., 1997. The human 37-kDa laminin receptor precursor interacts with the prion protein in eukaryotic cells. Nat. Med. 3, 1383–1388. https://doi.org/10.1038/nm1297-1383.

Riek, R., Hornemann, S., Wider, G., Billeter, M., Glockshuber, R., Wuthrich, K., 1996. NMR structure of the mouse prion protein domain PrP(121−231). Nature 382, 180–182. https://doi.org/10.1038/382180a0.

Ross, P.L., Huang, Y.N., Marchese, J.N., et al., 2004. Multiplexed protein quantitation in Saccharomyces cerevisiae using amine-reactive isobaric tagging reagents. Mol. Cell. Proteomics 3, 1154–1169. https://doi.org/10.1074/mcp.M400129-MCP200.

Rutishauser, D., Mertz, K.D., Moos, R., et al., 2009. The comprehensive native interactome of a fully functional tagged prion protein. PLoS One 4, e4446. https://doi.org/10.1371/journal.pone.0004446.

Sanghera, N., Pinheiro, T.J., 2002. Binding of prion protein to lipid membranes and implications for prion conversion. J. Mol. Biol. 315, 1241–1256. https://doi.org/10.1006/jmbi.2001.5322.

Santuccione, A., Sytnyk, V., Leshchyns'ka, I., Schachner, M., 2005. Prion protein recruits its neuronal receptor NCAM to lipid rafts to activate $p59^{fyn}$ and to enhance neurite outgrowth. J. Cell Biol. 169, 341–354. https://doi.org/10.1083/jcb.200409127.

Schmitt-Ulms, G., Legname, G., Baldwin, M.A., et al., 2001. Binding of neural cell adhesion molecules (N-CAMs) to the cellular prion protein. J. Mol. Biol. 314, 1209–1225. https://doi.org/10.1006/jmbi.2000.5183.

Schmitt-Ulms, G., Hansen, K., Liu, J., et al., 2004. Time-controlled transcardiac perfusion cross-linking for the study of protein interactions in complex tissues. Nat. Biotechnol. 22, 724–731. https://doi.org/10.1038/nbt969.

Schmitt-Ulms, G., Mehrabian, M., Williams, D., Ehsani, S., 2021. The IDIP framework for assessing protein function and its application to the prion protein. Biol. Rev. Camb. Philos. Soc. 96, 1907–1932. https://doi.org/10.1111/brv.12731.

Schwenke, K.A., Walzlein, J.H., Bauer, A., Thomzig, A., Beekes, M., 2022. Primary glia cells from bank vole propagate multiple rodent-adapted scrapie prions. Sci. Rep. 12, 2190. https://doi.org/10.1038/s41598-022-06198-4.

Scott, M., Foster, D., Mirenda, C., et al., 1989. Transgenic mice expressing hamster prion protein produce species-specific scrapie infectivity and amyloid plaques. Cell 59, 847–857. https://doi.org/10.1016/0092-8674(89)90608-9.

Sevillano, A.M., Aguilar-Calvo, P., Kurt, T.D., et al., 2020. Prion protein glycans reduce intracerebral fibril formation and spongiosis in prion disease. J. Clin. Invest. 130, 1350–1362. https://doi.org/10.1172/JCI131564.

Slapsak, U., Salzano, G., Amin, L., et al., 2016. The N terminus of the prion protein mediates functional interactions with the neuronal cell adhesion molecule (NCAM) fibronectin domain. J. Biol. Chem. 291, 21857–21868. https://doi.org/10.1074/jbc.M116.743435.

Telling, G.C., Scott, M., Mastrianni, J., et al., 1995. Prion propagation in mice expressing human and chimeric PrP transgenes implicates the interaction of cellular PrP with another protein. Cell 83, 79–90. https://doi.org/10.1016/0092-8674(95)90236-8.

Ulbrich, S., Janning, P., Seidel, R., et al., 2018. Alterations in the brain interactome of the intrinsically disordered N-terminal domain of the cellular prion protein (PrPC) in Alzheimer's disease. PLoS One 13, e0197659. https://doi.org/10.1371/journal.pone.0197659.

Walsh, D.J., Rees, J.R., Mehra, S., et al., 2024. Anti-prion drugs do not improve survival in novel knock-in models of inherited prion disease. PLoS Pathog. 20, e1012087. https://doi.org/10.1371/journal.ppat.1012087.

Watts, J.C., Huo, H., Bai, Y., et al., 2009. Interactome analyses identify ties of PrP and its mammalian paralogs to oligomannosidic N-glycans and endoplasmic reticulum-derived chaperones. PLoS Pathog. 5, e1000608. https://doi.org/10.1371/journal.ppat.1000608.

Watts, J.C., Stohr, J., Bhardwaj, S., et al., 2011. Protease-resistant prions selectively decrease Shadoo protein. PLoS Pathog. 7, e1002382. https://doi.org/10.1371/journal.ppat.1002382.

Watts, J.C., Giles, K., Stohr, J., et al., 2012. Spontaneous generation of rapidly transmissible prions in transgenic mice expressing wild-type bank vole prion protein. Proc. Natl. Acad. Sci. USA 109, 3498–3503. https://doi.org/10.1073/pnas.1121556109.

Watts, J.C., Giles, K., Patel, S., Oehler, A., DeArmond, S.J., Prusiner, S.B., 2014. Evidence that bank vole PrP is a universal acceptor for prions. PLoS Pathog. 10, e1003990. https://doi.org/10.1371/journal.ppat.1003990.

Watts, J.C., Giles, K., Bourkas, M.E., et al., 2016. Towards authentic transgenic mouse models of heritable PrP prion diseases. Acta Neuropathol. 132, 593–610. https://doi.org/10.1007/s00401-016-1585-6.

Watts, J.C., Bourkas, M.E.C., Arshad, H., 2018. The function of the cellular prion protein in health and disease. Acta Neuropathol. 135, 159–178. https://doi.org/10.1007/s00401-017-1790-y.

Williams, D., Mehrabian, M., Arshad, H., et al., 2021. The cellular prion protein interacts with and promotes the activity of Na, K-ATPases. PLoS One 16, e0258682. https://doi.org/10.1371/journal.pone.0258682.

Williamson, R.A., Peretz, D., Pinilla, C., et al., 1998. Mapping the prion protein using recombinant antibodies. J. Virol. 72, 9413–9418. https://doi.org/10.1128/JVI.72.11.9413-9418.1998.

Zafar, S., Shafiq, M., Younas, N., Schmitz, M., Ferrer, I., Zerr, I., 2017. Prion protein Interactome: identifying novel targets in slowly and rapidly progressive forms of Alzheimer's disease. J. Alzheimers Dis. 59, 265–275. https://doi.org/10.3233/JAD-170237.